SCIENTIFIC REPORTS

OPEN

SUBJECT AREAS:
HEPATITIS C VIRUS
VIRUS STRUCTURES

Received
2 December 2013

Accepted
13 March 2014

Published
1 April 2014

Stearoyl-CoA desaturase inhibition blocks formation of hepatitis C virus-induced specialized membranes

Rodney K. Lyn[1,2], Ragunath Singaravelu[1,3], Stacia Kargman[4], Shifawn O'Hara[1], Helen Chan[4]*, Renata Oballa[4]†, Zheng Huang[4]‡, Daniel M. Jones[5], Andrew Ridsdale[1], Rodney S. Russell[5], Anthony W. Partridge[4]§ & John Paul Pezacki[1,2,3]

[1]National Research Council of Canada, Ottawa, Ontario, Canada, [2]Department of Chemistry, Microbiology and Immunology, University of Ottawa, Ottawa, Canada, [3]Department of Biochemistry, Microbiology and Immunology, University of Ottawa, Ottawa, Canada, [4]Merck Research Laboratories, Merck & Co., Kenilworth, N.J., USA, [5]Immunology and Infectious Diseases, Faculty of Medicine, Memorial University of Newfoundland, St. John's, Newfoundland, Canada.

Correspondence and requests for materials should be addressed to A.W.P. (Anthony.Partridge@pharmaron.com) or J.P.P. (John.Pezacki@nrc-cnrc.gc.ca)

* Current address: Alexion Pharmaceuticals, Montreal, Canada.

† Current address: Inception Sciences Canada Inc., Vancouver, Canada.

‡ Current address: Eli Lilly China Research & Development Center, Shanghai, China.

§ Current address: Pharmaron, Beijing, China.

Hepatitis C virus (HCV) replication is dependent on the formation of specialized membrane structures; however, the host factor requirements for the formation of these HCV complexes remain unclear. Herein, we demonstrate that inhibition of stearoyl-CoA desaturase 1 (SCD-1) halts the biosynthesis of unsaturated fatty acids, such as oleic acid, and negatively modulates HCV replication. Unsaturated fatty acids play key roles in membrane curvature and fluidity. Mechanistically, we demonstrate that SCD-1 inhibition disrupts the integrity of membranous HCV replication complexes and renders HCV RNA susceptible to nuclease-mediated degradation. Our work establishes a novel function for unsaturated fatty acids in HCV replication.

Many viruses have evolved different mechanisms by which to alter the membrane components of the host-cell endoplasmic reticulum (ER) in order to form membranous structures that support viral replication[1–5]. Membrane alterations are observed with multiple classes of viruses exemplified by the Flaviviridae (e.g. hepatitis C virus (HCV), Coronaviridae (SARS), and Picornaviridae (polio virus))[3]. Virus-modified ER includes interconnected membranous structures that contain multiple single or double membrane invaginated piths, each housing and protecting viral replication complexes from host defences[3,6,7]. In the case of HCV, which chronically infects ~2.35% of the world's population[8], virus-induced piths/webs enable HCV RNA to hide from endogenous host defenses[3]. Further, hepatic lipid droplets (LDs) bound to the HCV core protein also blocks access to host defences[9]. Finally, the high radii of curvature of HCV-induced modified ER membranes provides a platform for replication and concentrates viral components for protection and efficiency[3,10,11]. Small molecules that inhibit host and viral proteins governing formation of these virus-modified membranes can serve as chemical probes to study the roles of these protected environments and also represent novel antiviral strategies.

Herein we examined a series of stearoyl-CoA desaturase 1 (SCD-1) inhibitors as probes for HCV-induced membrane alterations. We report that SCD-1 inhibition potently represses HCV replication by disrupting the formation of membranous webs and rendering HCV RNA susceptible to nuclease-mediated degradation. Our work demonstrates that unsaturated fatty acids play a crucial role in HCV-induced changes in membrane morphology required for efficient viral replication.

Results

Membrane curvature in phospholipid bilayers can be altered through their fatty acids compositions. Specifically, the nature of fatty acids have been shown to affect the packing of phospholipid fatty-acyl chains, inducing either positive or negative curvature, depending on the structure and size of the lipid and fatty acid head group[12,13]. For example, oleic acid (OA) augments membrane fluidity in physiologically relevant phospholipid membrane bilayers and also enables negative curvature[14]. As such, we examined the effects of oleic acid and its involvement in HCV-induced negatively curved membranes. A key enzyme in the biosynthesis of oleic acid is stearoyl-CoA desaturase (SCD)[15]. In humans, SCD-1 is highly expressed in the liver, while the other isoform, SCD-5 is primarily expressed in the brain and pancreas[15,16]. SCD introduces a *cis* double bond in a highly specific manner at the Δ9

position of long-chain acyl-CoAs, with greater selectivity for palmitoyl- and stearoyl-CoA[15]. The monounsaturated fatty acid (MUFA) products of SCD-1 enzymatic activity are shuttled as substrates for the synthesis of membrane phospholipid fatty-acyl chains, triglyceride biogenesis, and cholesterol esterification (Fig. 1)[12,17,18]. A variety of small molecule inhibitors have been used to show that inhibiting lipogenesis negatively affects HCV replication[19]. To determine whether HCV replication is dependent on SCD-1 activity, we treated human hepatoma cells (Huh7) stably expressing an HCV replicon with the SCD-1 inhibitor **A**[20] (Fig. 2). Dose dependent reduction of viral RNA replication was observed following 96 hr treatments with inhibitor **A** (EC_{50} = 62 nM, Fig. 2c). No toxicity was observed at all concentrations tested (Supplementary Fig. S1). A panel of other previously characterized SCD-1 inhibitors, representing distinct

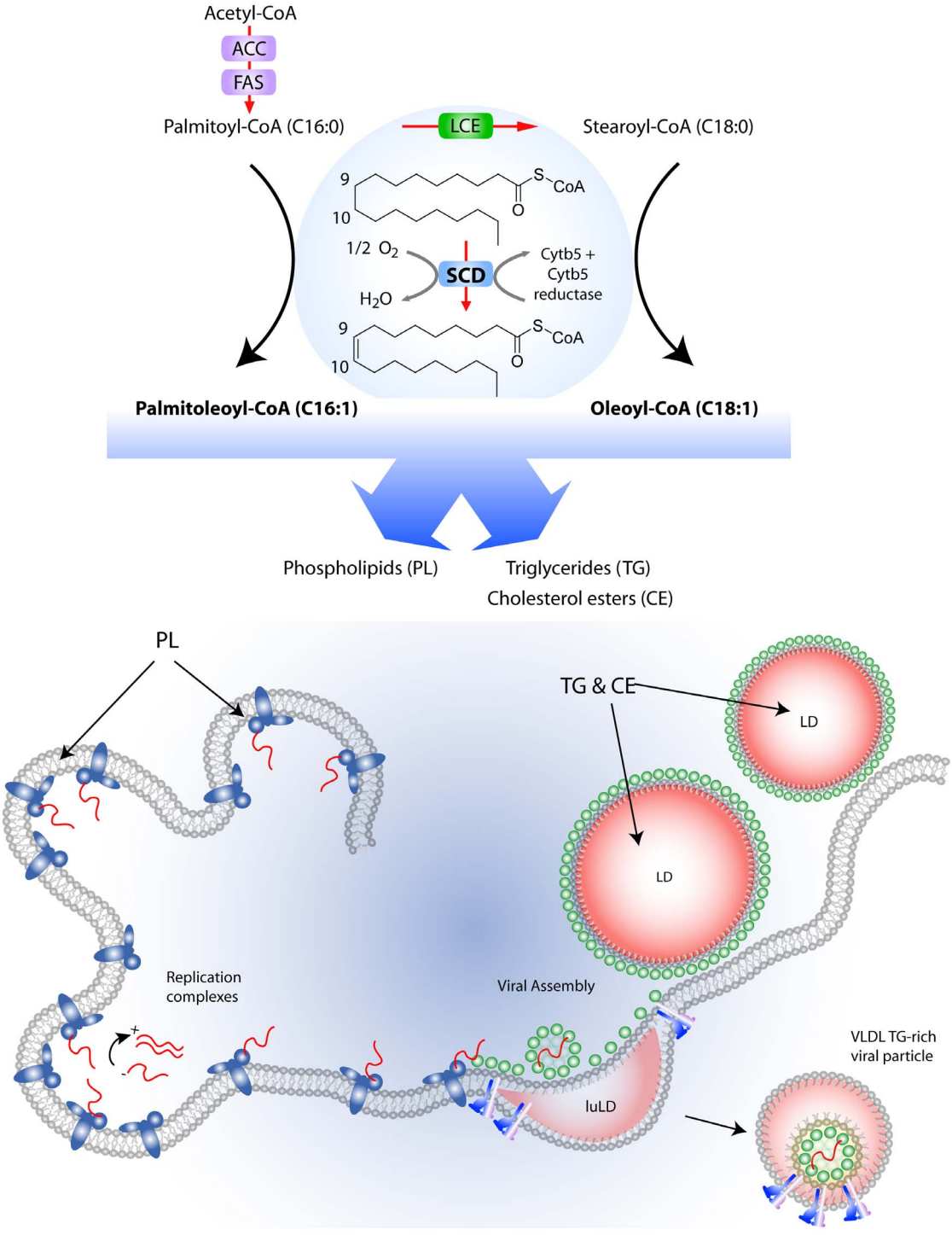

Figure 1 | Role of SCD-1 in the fatty acid biosynthesis pathway. Multiple enzymes, that include acetyl-CoA carboxylase (ACC) and fatty acid synthase (FAS), catalyze the conversion of acetyl-CoA into long chain fatty acids (LCFAs). Palmitoyl-CoA (C16:0) can undergo sequential long-chain elongation (LCE) to form stearoyl-CoA (C18:0). Both of these fatty acids represent substrates for SCD-1, which catalyzes their desaturation at carbon-9 forming a cis-double bond. The SCD-1 catalyzed products, palmitoleoyl-CoA (C16:1) and oleoyl-CoA (C18:1), are directly incorporated in triglycerides (TGs), cholesterol esters (CEs), and phospholipids (PL). These lipids are crucial to the formation of cytosolic lipid droplets (cLDs), luminal LDs (luLD), and lipid-rich membranes, which are platforms for HCV replication and assembly.

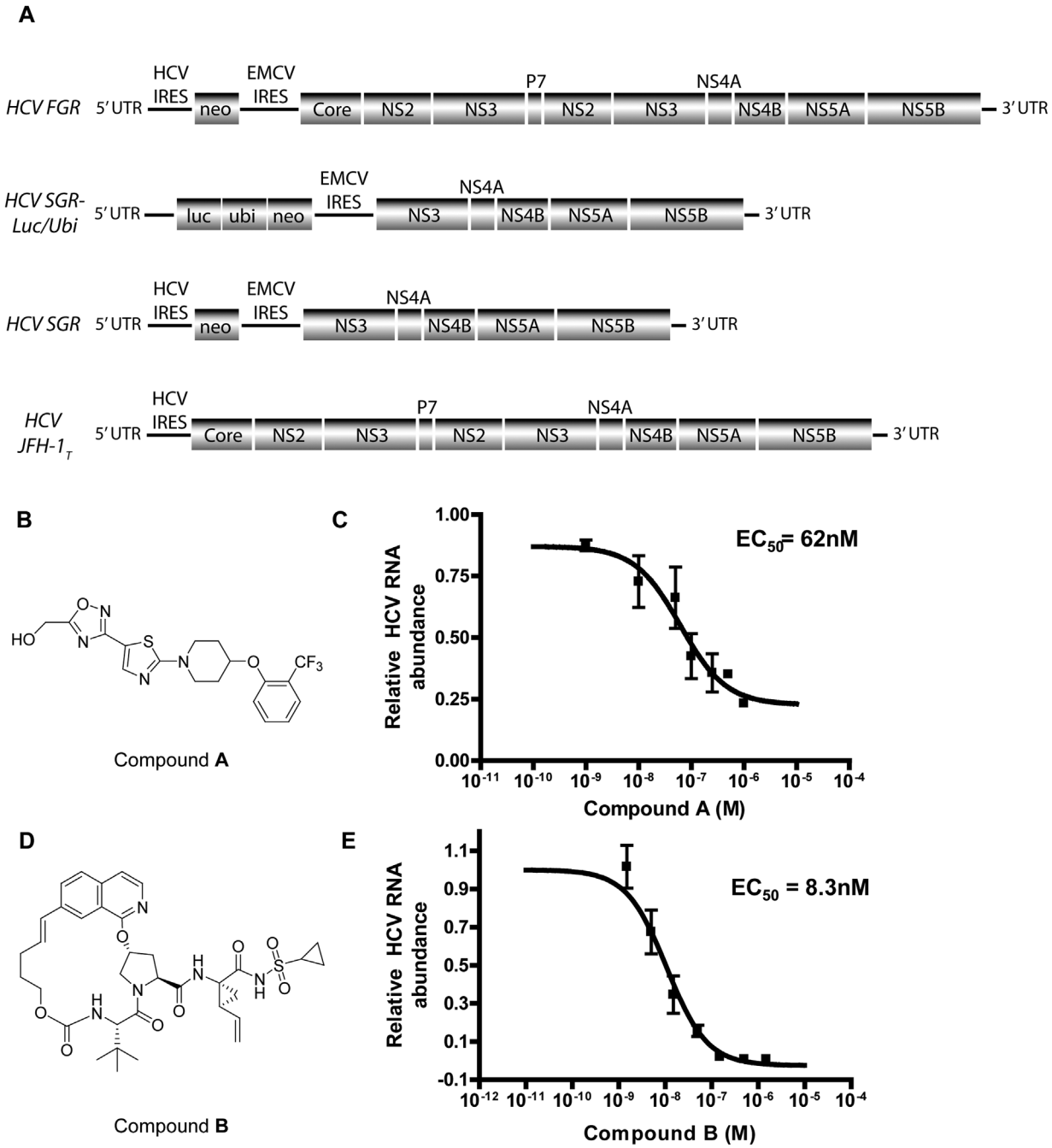

Figure 2 | SCD-1 inhibition represses HCV replication. (A) A schematic depicting the full genomic replicon (FGR), subgenomic replicons (SGR), and full-length virus (JFH-1_T) used in this study. All replicons encode for a neomycin (neo) resistance gene used as a selectable marker, and expression of HCV polyprotein is driven by encephalomyocarditis (EMCV) internal ribosomal entry site (IRES). All replicons are flanked by the HCV 5′ untranslated region (UTR) and 3′UTR. Both SGRs encode for NS3-NS5B. HCV SGR-Luc/Ubi (genotypes 1A and 1B) also encodes a luciferase reporter tag (luc) followed by a ubiquitin (ubi) gene. (B) Chemical structure of SCD-1 thiazole analogue inhibitor **A**. (C) Huh7 cells stably expressing HCV-SGR (genotype 1B) were treated with varying concentrations of the SCD inhibitor **A**. Quantitative real-time PCR (qRT-PCR) performed on RNA isolates 96 hours post-treatment demonstrates a decrease in HCV RNA levels induced by inhibiting SCD-1 in a dose-dependent manner. The error bars represent standard error of the mean ($n \geq 3$). (D) Chemical structure of NS3 protease inhibitor **B**. (E) A dose response curve of HCV inhibition by inhibitor **B** after a 96 hour treatment in Huh7.5 cells stably expressing HCV-FGR (genotype 1B). RNA levels were analyzed as in (C).

structural classes[20–24], were also tested against genotype 1a and 1b HCV replicons, with EC_{50} values for inhibition of viral replication measured as low as 0.74 nM (Supplementary Table S1). Inhibition by the SCD-1 inhibitors compared well with the direct-acting antiviral (DAA) inhibitor **B**[25] that inhibits HCV NS3 protease with an EC_{50} value of 8.3 nM (Fig. 2e). In some cases SCD-1 inhibitors (Supplementary Table S1) blocked HCV replication to a low level but did not abolish all replication as seen in DAA treatments, indicating a different mechanism of action for the SCD-1 inhibitors as demonstrated by a lack of inhibitory effect on *in vitro* NS3 protease and NS5B polymerase activity (Supplementary Table S2). Similar levels of inhibition of HCV replication and virus production were observed in a full-length genotype 2a (JFH-1_T)[26] model (Fig. 3). These results suggest that SCD-1 activity is highly advantageous

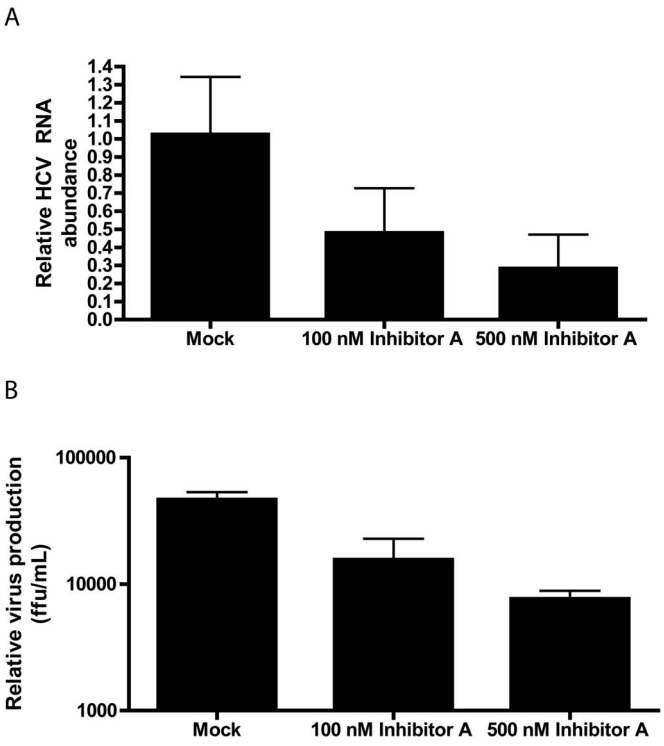

Figure 3 | SCD-1 inhibition represses full-length HCV replication and infectivity. Huh7.5 cells were infected with JFH-1_T HCV (MOI = 0.1). 24 hours post-infection, infected cells were treated with varying concentrations of inhibitor **A** (mock, 100 nM or 500 nM). 120 hours post-treatment, intracellular HCV RNA levels were profiled via qRT-PCR (A). Supernatants were used to infect naïve Huh7.5 cells, and titres were measured (B). Viral titres are expressed as the number of focus-forming units (FFU) per ml of supernatant. Error bars represent standard deviation of the mean ($n \geq 2$).

for HCV replication and pharmacological inhibition of SCD-1 leads to an antiviral effect similar to DAAs.

To confirm the specificity of the effect, we utilized a ^{14}C isotope method to directly measure SCD-1 inhibitory effect of our panel of SCD inhibitors in Huh7 cells harboring HCV replicons (Supplementary Fig. S2). We observed strong correlation between HCV inhibition and SCD-1 inhibition within these cells suggesting that the antiviral properties of our SCD inhibitors are due to on-target inhibition of the SCD-1 enzyme (Fig. 4). The specificity was further demonstrated by the ability of OA addition to rescue the antiviral effects of the SCD inhibitors (Supplementary Table S1). Finally, SCD inhibitors had no observed effect on HIV replication/spread in a cellular assay. Taken together, these data suggest that inhibitor **A** acts to block HCV replication by reducing OA levels and that this effect is specific for HCV.

To investigate how SCD inhibitors block HCV replication, we initially focused on their effects on LDs since neutral lipids that form triglycerides and cholesterol esters are the major components of LDs[27]. Because MUFAs such as OA are highly incorporated into triglycerides, it is conceivable that there would be a reduction in storage of these neutral lipids in LDs upon SCD-1 inhibition[15]. Thus, we treated Huh7 cells, with and without a HCV subgenomic replicon, with the SCD-1 inhibitor **A** at concentrations ranging from 1 nM to 1 μM. We then performed cellular imaging using coherent anti-Stokes Raman scattering (CARS) microscopy, a label-free method for LD detection[28,29] and voxel analysis, which quantifies lipid volumes from the threshold CARS signal specific for LDs[30]. We detected a small change in LD density when Huh7 cells stably expressing an HCV subgenomic replicon were treated with concentrations well above the EC_{50} value for inhibitor **A** (Fig. 5). The LD size and cellular distribution did not change in cells treated with inhibitor **A** below 250 nM. This indicates that there is no appreciable reduction in LD size or density at concentrations of SCD-1 inhibitor that can cause inhibition of HCV replication. At concentrations above 250 nM, we observed a significant reduction in cellular lipid content. Our observations were specific for SCD-1 inhibitor **A**[20] as treatment with inhibitor **B**[25], which targets the NS3 protease, produced no discernible changes in LDs across all concentrations of inhibitor (Supplementary Fig. S3).

As our CARS imaging data suggested that inhibitor **A** mediated repression of HCV occurs prior to any detectable effect on LDs, we considered alternative mechanisms. Specifically, we postulated that the pharmacological blockade of SCD-1 would alter membrane composition, fluidity and/or the curvature required for functional HCV replication complexes. To test this hypothesis, we assessed the cellular localization of double-stranded (ds) HCV RNA, a species normally localized to intact replication complexes, upon treatment with varying concentrations of SCD inhibitor **A** (Fig. 6). Using an antibody specific for dsRNA[30] and Huh7 cells stably transfected with HCV replicons, confocal microscopy revealed that in untreated cells, ds-HCV RNA exhibits a punctate staining pattern within the cytoplasmic space of the cell (Fig. 6a). Under mock treatment, a similar punctate pattern was also observed, as expected (Fig. 6b). However, upon addition of 100 nM of SCD-1 inhibitor **A**, we detected a diffuse dispersion pattern of ds-HCV RNA intermediates that are consistent with a significant change in localization (Fig. 6c). We reasoned that the exclusion of ds-HCV RNA from HCV-modified membranes caused the down-regulation of HCV replication since the RNA is no longer protected from endogenous nucleases and is likely no longer associated with host and viral proteins that mediate replication, as previously reported[30]. This is consistent with SCD inhibitor **A** affecting HCV modified membranes.

Next, we sought to further examine the possibility that inhibitor **A** is disrupting HCV-induced modified membranes through SCD-1 inhibition and the depletion of intracellular MUFAs. Previous studies demonstrated that HCV RNA in replication complexes is nuclease resistant[31]. On the molecular level, the replication complex membranes have high curvature that is likely induced at least in part by oleic acid-derived phospholipids. These membranes are characterized by their detergent and nuclease resistant properties[9,31,32]. Therefore, inhibiting SCD-1 may modulate the properties of the replication complex, rendering HCV RNA susceptible to the endogenous nucleases that are employed by the cell as a cellular defense mechanism.

To examine this possibility, we performed an *in situ* RNAse protection assay (RPA) based on a previously published methodology[9,31]. Miyanari *et al.* showed previously that HCV RNA in replication complexes remains intact in the presence of a membrane permeabilizing detergent (digitonin) and exogenous nucleases[9,31]. However, upon disruption of the ER membrane integrity using an additional non-ionic detergent (NP-40), HCV RNA became susceptible to nuclease-mediated degradation. We sought to investigate whether inhibitor **A** exerts a similar effect on the structural integrity of HCV altered membranes as NP-40, by inhibiting SCD-1 and lowering oleate levels. This is consistent also with the ability of oleic acid to rescue the effect (Supplementary Table S1). We performed comparative PCR for HCV RNA levels followed by densitometry to quantify the magnitudes of HCV RNA degradation after probing for nuclease accessibility to HCV RNA (Fig. 7, and Supplementary Fig. S4). The RPA was performed during mock (Fig. 7a,b lanes 1–6) and SCD-1 inhibitor **A** (Fig. 7a,b lanes 7–11) treatments to examine the influence of SCD-1 on the nuclease and detergent resistant properties of viral RNA at replication complexes. Cells were treated at a concentration yielding ~50% reduction of HCV RNA by PCR ($n = 5$) (Fig. 7b,c and Supplementary Fig. S4). This was performed

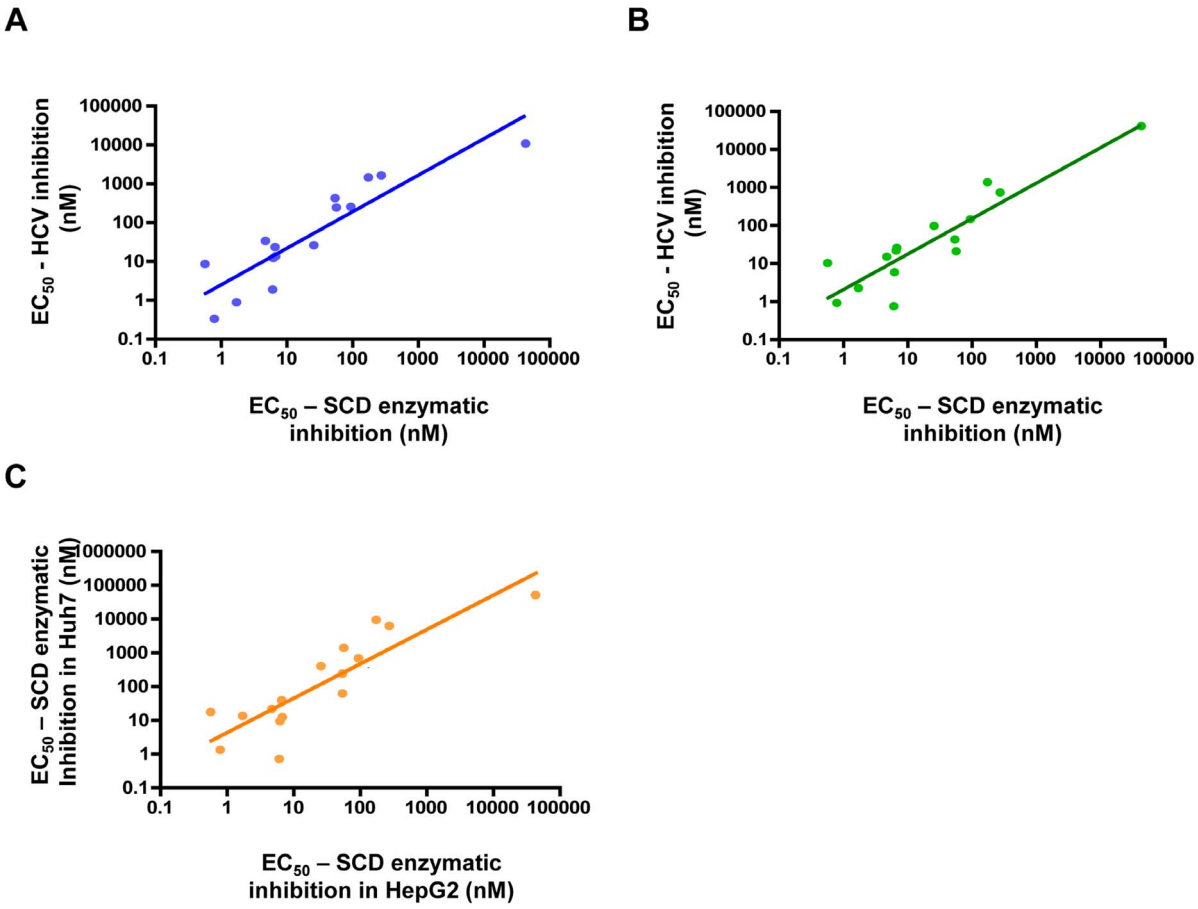

Figure 4 | Correlation between antiviral activity and SCD-1 inhibition. HCV replication was measured in HCV SGR-Luc/Ubi Huh7 cells expressing HCV (A) genotype 1B or (B) genotype 1A upon treatment with different SCD-1 inhibitors (described Table S1) via luciferase assays. In parallel, the cell-based enzymatic activity of SCD-1 was measured, as described in Materials and Methods. (A–B) For each inhibitor, the EC_{50} of HCV inhibition is plotted against the EC_{50} of SCD-1 inhibition. (C) HepG2 cells were similarly treated with each SCD-1 inhibitor, and EC_{50} of SCD-1 inhibition in HepG2 cells is plotted against the respective EC_{50} of SCD-1 inhibition in Huh7 SGR-Luc/Ubi cells.

to ensure that we would be able to observe additional reduction of HCV RNA levels by endogenous and exogenously added nucleases. 28S and 18S ribosomal RNAs are susceptible to degradation by cytoplasmic nucleases, and their degradation is a positive control for both cell membrane permeabilization and nuclease activity (Fig. 7a,b). As expected, in treatments containing both nuclease and digitonin, 28S and 18S rRNA are readily degraded (Fig. 7a,b, lanes 3 and 9), whereas HCV RNA is not. In the absence of digitonin, the exogenous nuclease fails to enter the cytoplasm, and as expected, no degradation is observed (Fig. 7a,b, lane 6). Additionally, when NP-40 was added in the absence of nuclease and digitonin, ribosomal RNAs remained intact (Fig. 7a,b, lanes 4 and 10). SCD-1 inhibition alone has no effect on the integrity of ribosomal RNA bands (Fig. 7a,b, lane 7). Interestingly, we observed that for digitonin and nuclease treated cells, inhibitor **A** (Fig. 7a,b, lane 9) reduced HCV RNA levels similar to the effects of NP-40 (Fig. 7a,b, lane 5). This suggests that the SCD-1 inhibitor disrupts the structural integrity of HCV modified membranes to a similar extent to that of NP-40, which allows exogenous nucleases access to HCV RNA. For inhibitor **A** as well as digitonin plus nucleases treated cells, the HCV RNA levels showed above 50% reduction in HCV RNA levels (See Fig. 7a,b, lane 8 vs 9). This further supports the notion that SCD-1 inhibitor treated HCV replicon containing cells are more susceptible to nucleases where SCD-1 inhibitor-induced membrane perturbation allows nuclease access into the replication complexes to degrade HCV RNA to a greater extent than mock treated cells. After repeating the exogenous nuclease protection assay (n = 5), we observed that HCV RNA levels in digitonin, nuclease, and inhibitor **A** treated HCV replicon containing cells showed no statistically significant difference in comparison to digitonin, nuclease, and NP-40 treatment, which further confirms that the effects of inhibitor **A** mimic NP-40 treatment in disrupting the protective environment of the membranous webs (Fig. 7c). As expected, no significant degradation of HCV RNA was observed in cells treated with digitonin only (Fig. 7a,b, lane 1), NP-40 only (Fig. 7a,b, lane 4), and nuclease only (Fig. 7a,b, lane 6), in both mock and SCD-1 inhibitor **A** (Fig. 7a,b, lanes 8 and 10) treated groups. Ultimately, the RPA demonstrates that reduced oleate from SCD-1 inhibitor treatment caused a change in the nuclease resistant HCV replication complexes, which then become accessible to endogenous or exogenously added nucleases.

Finally, we performed electron microscopy (EM) of Huh7 SGR cells treated with inhibitor **A**. We found that at a dose of 100 nM there was a significant decrease in the numbers of membranous webs, consistent with HCV knockdown, and a dramatic change in the structure of the membranous webs (Fig. 8). Specifically, double membrane vesicles, a proposed site of HCV replication, displayed a distorted morphology (Fig. 8c,f) and increased prevalence of small vesicles was observed. Collectively, these observations are consistent with SCD inhibition altering and ultimately blocking the formation HCV-induced specialized membranes. EM imaging of Huh7 SGR cells at a dose of 500 nM showed almost no membranous webs and drastically fewer LDs compared with control cells (Supplementary Fig. S5), consistent with our observations using CARS microscopy (Fig. 5).

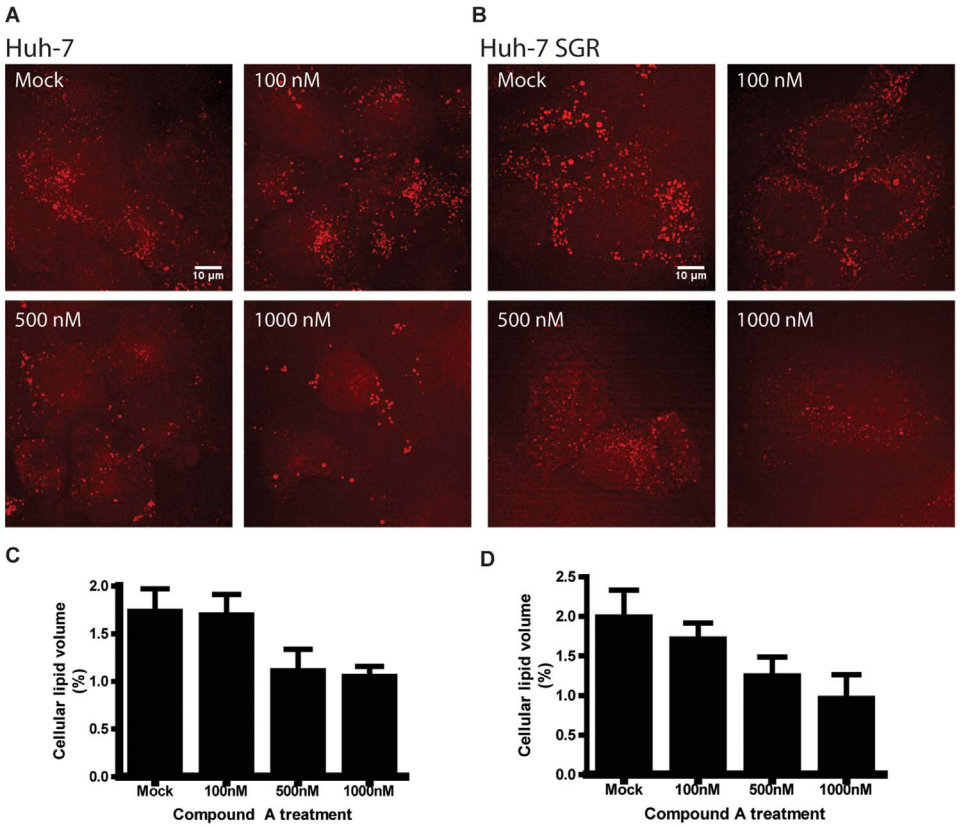

Figure 5 | Inhibitor A's antiviral inactivity is independent of any effect on cytosolic lipid droplets. (A) Huh7 and (B) Huh7-SGR cells were treated with a concentration range of inhibitor **A** (Mock; 100–1000 nM) and imaged by CARS microscopy. Representative images are shown (n = 2). Scale bar = 10 μm. The percentage LD volume was measured by voxel analysis for multiple cells (n > 10) under multiple field of views for each concentration, and the results for (C) Huh7 and (D) Huh7-SGR cells are depicted in the bar graphs shown. Error bars shown represent the standard error of the mean.

Discussion

HCV, like other viruses, partitions its genome into membranous compartments in order to increase viral replication kinetics and shield the viral genome[33,34]. However, our current understanding of the biogenesis of HCV-associated membranous webs is limited. While it is well established that HCV hijacks host lipid homeostasis to facilitate its pathogenesis[19,35,36], there is an emerging body of evidence that these lipid pathways play an important role in HCV's formation of membranous replication complexes. This includes the modulation of phosphoinositide signaling and cholesterol synthesis to induce the formation of the HCV replication compartments[2,37]. Previous work analyzing the role of fatty acid biosynthesis in HCV pathogenesis has had a central focus on its relevance in HCV-induced hepatic lipid accumulation. Our study demonstrates an important role for unsaturated fatty acids in the formation of HCV-induced membranous compartments.

Our findings provide a new context for previous research investigating fatty acids' role in HCV pathogenesis. Earlier work demonstrated that HCV activates SREBP-1C and PPAR-γ activity to activate fatty acid biogenesis[16,38,39]. Separate studies report HCV inhibits PPAR-α activity to decrease fatty acid catabolism[40–42]. This HCV-induced increase in cellular fatty acid levels may serve as a source of unsaturated fatty acids for formation of the viral replication complex. Our proposed pro-viral role of SCD-1 is consistent with recent studies demonstrating HCV activates SCD expression and activity[38,43,44]. Conversely, our data highlights an additional potential anti-viral mechanism of action for inhibitors of fatty acid synthesis previously reported to repress the HCV viral life cycle[45–47], through downstream modulation of unsaturated fatty acid levels, such as is the case for inhibitor **A**.

Overall, we have established inhibitor **A** as a probe for oleic acid-dependent membrane environments. We have shown that inhibiting SCD-1 decreases HCV RNA replication, through compromising the integrity of the membrane environment at replication complexes. Also, we demonstrated that SCD-1 inhibition increases the susceptibility of HCV RNA to exogenous nucleases in permeabilized cells suggesting that SCD-1 inhibition disrupts oleic acid-induced negative membrane curvature. To the best of our knowledge, this is the first direct evidence of unsaturated fatty acids playing a role in the formation of HCV replication complexes. Finally, given the recent development of liver-targeted SCD inhibitors[48], SCD-1 inhibition represents a novel host-targeted therapeutic strategy for the treatment of HCV infection.

Methods

Cell culture and reagents. Human hepatoma cells (Huh7) cells harboring the pFK-I389neo/NS3-3′/5.1 subgenomic replicon (Huh7 SGR; genotype 1b) and Huh7.5 cells stably expressing the full-length HCV genotype 1b replicon with a S2204I adaptive mutation in NS5A (Huh7.5 FGR) were maintained in DMEM medium supplemented with 100 nM nonessential amino acids, 50 U/mL penicillin, 50 μg/mL streptomycin, and 10% FBS (CANSERA, Rexdale, ON), and 250 μg/mL G418 Geneticin (GIBCO-BRL, Burlington, ON). Huh7 cells co-expressing genotype 1a or 1b and luciferase reporter were grown in complete DMEM media containing 0.25 mg/ml G418 antibiotic and supplemented with 10% fetal bovine serum, non-essential amino acids, penicillin/streptomycin, L-Glutamine, and Sodium pyruvate.

Huh7 cells harboring the genotype 1a or 1b replicon and the neomycin resistance gene were grown in complete DMEM media containing 0.25 mg/ml G418 antibiotic and supplemented with 10% fetal bovine serum, non-essential amino acids, penicillin/streptomycin, and L-Glutamine.

The pFK-I389neo/NS3-3′/5.1 subgenomic replicon was kindly provided by Ralf Bartenschlager (Institute of Hygiene, University of Heidelberg, Germany). The Huh7.5 FGR cell line was a kind gift from Dr. Charles M. Rice (Rockefeller University, New York, USA) and Apath LLC (St. Louis, MO, USA). The JFH-1_T HCV strain harbors 3 amino acid mutations which enhance infectious virus production. The

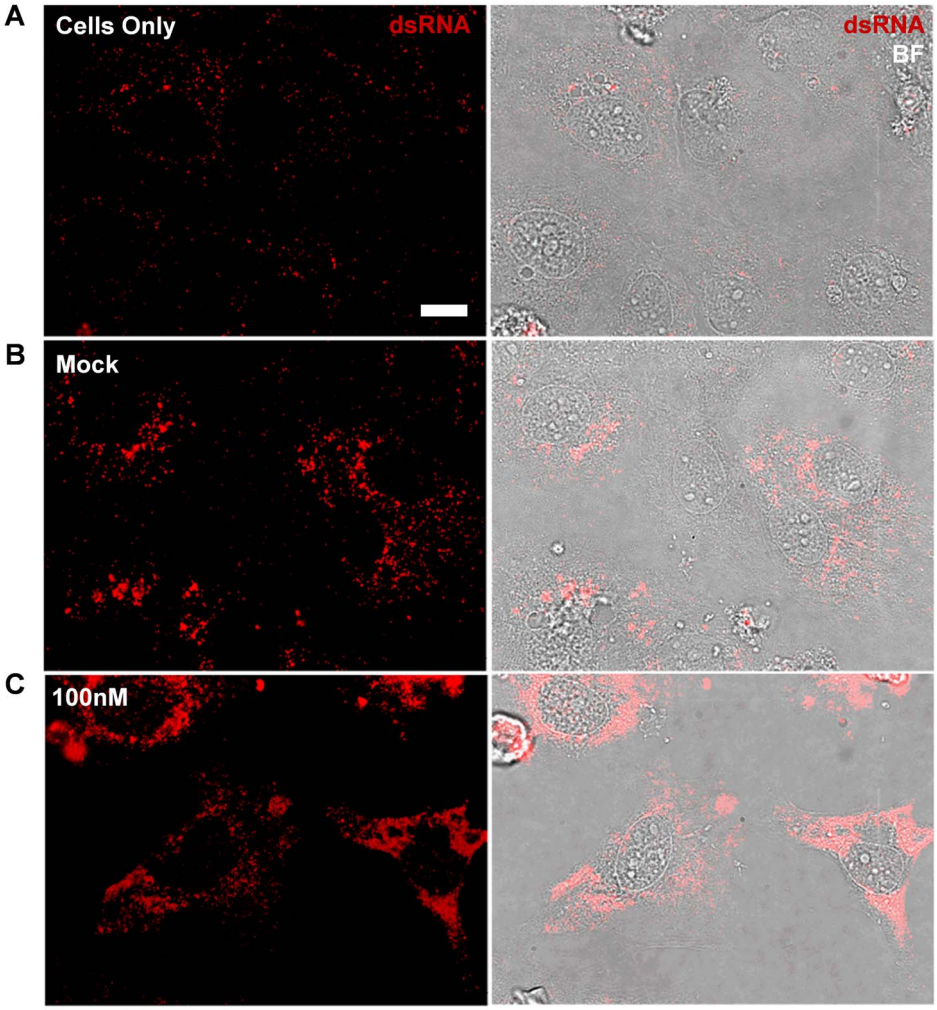

Figure 6 | SCD-1 inhibition induces dispersion of ds-HCV RNA. Ds-HCV RNA intermediates using immunofluorescence in Huh7-SGR. Bright field images are also included to show distinct nuclei. Control samples, (A) cells only and (B) mock, showed high levels of punctate staining throughout the cell but with higher concentrations in the perinuclear region. The inhibitor **A** treatments at (C) 100 nM showed a more diffuse pattern suggesting that these dsRNA-intermediates are not localized in the functional replication complexes as a result of dispersion away from these complexes. Scale bar = 10 μm. Results are representative of two biological replicates.

strain was derived from the cell culture-adapted JFH-1 strain JFH-AM1, as previously described[26].

SYBR Green-based quantitative RT-PCR. Dose response curves were performed using Huh7-SGR cells for inhibitor **A** and Huh7.5-FGR cells for inhibitor **B**. At cell confluency between 20–30% in 6-well plates, cells were treated with serial dilutions of inhibitor **A** (1 mM–10 nM) or inhibitor **B** (1 mM–10 nM) or DMSO (mock) and incubated for 96 hours. RNA isolation from hepatocytes was performed using TriZol (Invitrogen) as per the manufacturer's protocol. RNA integrity was confirmed by electrophoresis on 0.8% agarose gel in 1× TBE (Ambion, Austin, TX). 250 ng of total RNA was reverse transcribed into cDNA using the Superscript II Reverse Transcriptase kit (Invitrogen, Carlsbad CA). Quantitative PCR (qPCR) of HCV and 18S rRNA levels was performed on an iCycler (Bio-Rad, Hercules, CA) using iQ SYBR Green Supermix (Bio-Rad,), as per manufacturer's protocol. The primer sequences are described in Supplementary Table S3. A 20 μL reaction was assembled according to the manufacturer's protocol. For data analysis, the $2^{-\Delta\Delta Ct}$ method was used, and mean fold changes in expression are shown relative to mock or control transfected samples[49].

Luciferase assay. HCV replication was measured in Huh7 cells expressing an HCV replicon and a luciferase reporter essentially as described previously[50]. Cells were harvested by trypsinization, quenched with complete media with G418, filtered through a 70 μm cell strainer, and then resuspended in complete FBS media (without G418) or complete media supplemented with 50% normal human serum (NHS, without G418). Cells were plated at 30 μl/well and at 2000 cells per well (FBS media) or 4000 cells per well (NHS media) in white 384 wells plates (Costar, 3570) using a Biomek FX with a 384 well head. Plates were left at room temperature for 30 min at which point 150 nL compound at various concentrations or DMSO, as a control, was added using the Echo 555 acoustic liquid handler followed by incubation at 37°C, 5% CO_2. After 72 hours, cells were allowed to equilibrate to room temperature prior to addition of Bright-Glo luciferase substrate (Promega E220). Following a 5 minute incubation at room temperature in the dark, luminescence (correlated with RNA replication) was detected using an Envision Multilabel plate reader (Perkin Elmer). For rescue experiments, media was supplemented with palmitoleic or oleic acid. Prior to cell treatment, stocks of oleic or palmitoleic acid in 100% ethanol were added to DMEM media (final concentration of palmitoleic/oleic acid of 100 μM, final ethanol concentration of 0.1 to 0.2%) and were sonicated in a water bath for 5 min at room temperature. Rescue experiments were performed for 72 hours in the presence of SCD inhibitors.

Taqman-based quantitative RT-PCR. Viral replication was measured in Huh7 cells harboring the genotype 1a or 1b replicon and the neomycin resistance gene as described previously[51]. Cells were harvested using 0.25% trypsin-EDTA, and resuspended in complete FBS media (without G418) or complete media supplemented with 50% normal human serum (NHS). Replicon cells were plated at 8000 cells per well in a 96-well plate in 100 μl of Complete Media (-G418) and incubated at 37°C with 5% CO2. Twenty-four hours later, 25 μl of compound or DMSO control in complete media (without G418) containing 1% DMSO was added to each well and the plates were incubated at 37°C, 5% CO_2. Seventy-two hour later, replicon RNA was isolated using RNeasy 96 well kit (Qiagen, Mississauga, Ontario) according to the manufacturer's instructions, and quantitated using real-time polymerase chain reaction (qRT-PCR) with the EZ RT-PCR kit (Applied Biosystems, Foster City, CA). The following primer/probes were used as a measure of HCV replication: Neo Forward [10 μM] CCG GCT ACC TGC CCA TTC; Neo Reverse [10 μM] CCA GAT CAT CCT GAT CGA CAA G; Neo Probe [5 μM] FAM-ACA TCG CAT CGA GCG AGC ACG TAC-Tamra. A commercially available primer/probes set for the cyclophilin gene (Taqman PDAR Human Cyclophilin (20×) (Applied Biosystems) was used to control for well-to-well variations.

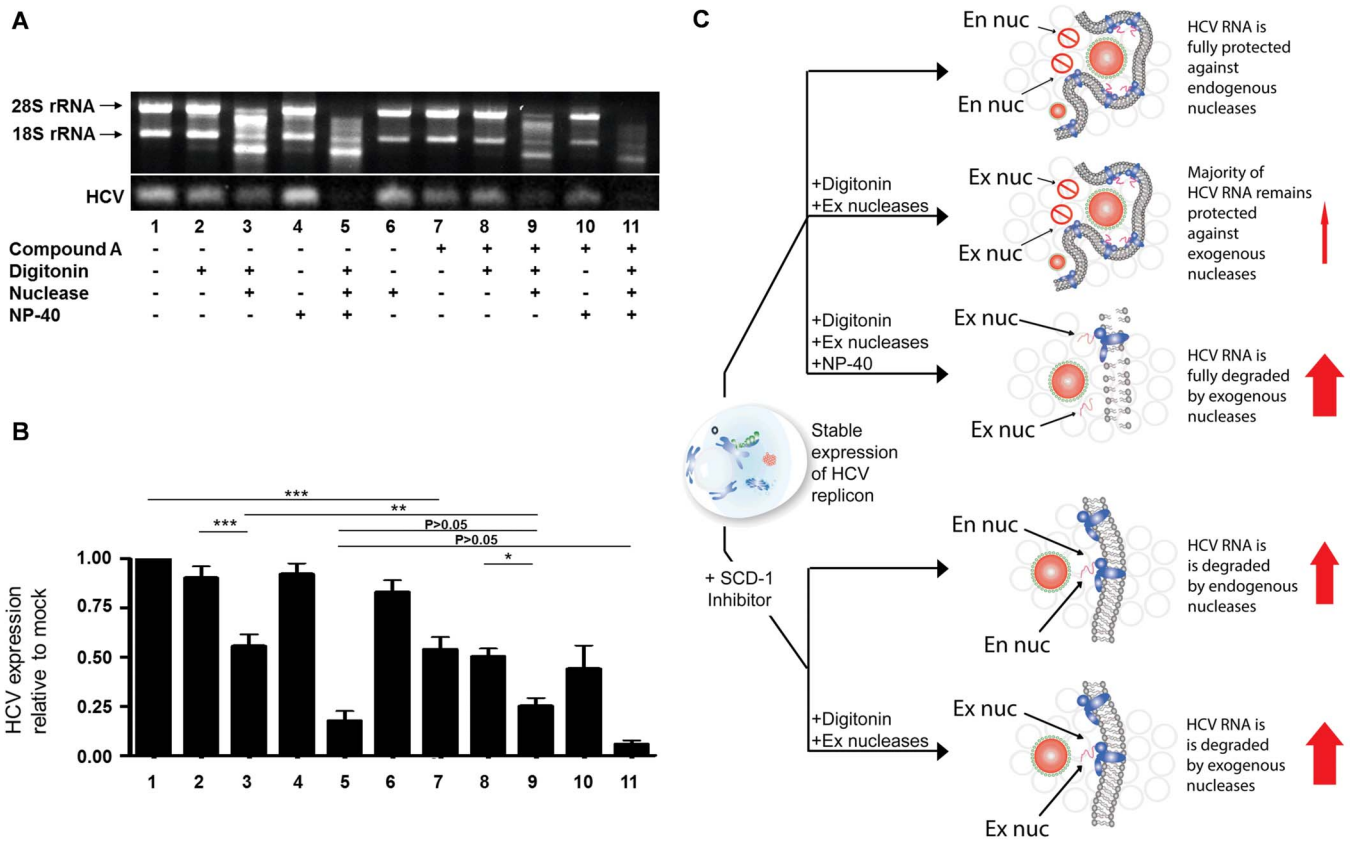

Figure 7 | SCD-1 inhibition increases HCV RNA susceptibility to exogenous nucleases. (A) Huh7-SGR cells were treated with vehicle (DMSO) (Lanes 1–6) or inhibitor **A** (Lanes 7–11) at a concentration yielding a 50% reduction in HCV RNA levels. 96 hours post-treatment, samples were treated with a combination of digitonin (Lanes 2, 3, 5, 8, 9, 11) micrococcal nuclease (Lanes 3, 5, 6, 9, 11) or NP-40 (Lanes 4, 5, 10, 11). A representative integrity gel is shown (n = 5) illustrating 18S and 28S ribosomal RNA integrity after digitonin, micrococcal nuclease, and NP-40 treatments. Degradation of 18S and 28S rRNA bands is observed only upon permeabilizing the plasma membrane with digitonin, and treatment with exogenous micrococcal nuclease (Lanes 3, 5, 9, 11). Comparative RT-PCR was performed on HCV RNA to illustrate the relative HCV RNA abundance (cropped image below the RNA integrity gel) in the presence and absence of inhibitor **A** after treatments with digitonin, micrococcal nuclease, and NP-40. (B) Average HCV RNA abundance is shown from comparative PCR detecting HCV RNA. Densitometry was performed to calculate the HCV RNA abundance. All values were normalized by Lane 1 (no treatment). (C) Schematic model for SCD-1 inhibition-mediated disruption of HCV replication. Inhibition of SCD-1 alters HCV RNA's susceptibility to exogenously added nucleases by disrupting membrane HCV-associated membranes at the replication complexes. Multiple models are depicted for HCV RNA's susceptibility to endogenous nucleases (En nuc) and exogenous nucleases (Ex nuc). The size of the red arrow represents the magnitude of HCV RNA degradation by endogenous and exogenous nucleases under the different treatments including digitonin, micrococcal nucleases, and/or NP-40.

Cell-based HIV replication assay. HIV replication was measured using a multi-cycle HIV replication assay and wild-type virus. Viral replication was determined by measuring HIV-1p24 gag antigen using the AlphaLISA technology (Perkin Elmer) after lysis of cells and viruses. MT-4 cells were maintained at a density of 0.1–3 million cells/mL in RMPI media supplemented with 10% FBS, L-glutamine, and Pen/Strep (10,000 IU/mL Pen and 10,000 ug/mL Strep). Virus was diluted in RPMI containing 10% FBS. MT-4 cells were washed in serum free medium, resuspended in medium containing virus at 250,000 cells/ml and incubated for 24 hours at 37°C and 5% CO_2 for 24 hours. Bulk-infected cells were washed in serum free media, resuspended in complete medium at 400,000 cells/ml and added to 384 TC-treated clear polystyrene plates (Costar 3701) at 30 µl per well. 30 µl of complete media containing inhibitor or DMSO were added the assay plates (final DMSO concentration of 0.25%) and incubated at 37°C and 5% CO_2. After 72 hours, cells were lysed, and incubated with acceptor (Anti-HIV p24 gag AlphaLISA Acceptor beads (5 mg/mL) (Perkin Elmer custom preparation CUSM73518000EA; Ref# 73518) and donor beads (Perkin Elmer 6760002) according to the manufacturer's instructions. Plates were incubated for 60 minutes at room temperature in the dark followed by signal detection using a Pherastar plate reader.

NS3 protease activity - time-resolved fluorescence assay. NS3 protease activity was measured essentially as described previously[52] using the full length NS3/4A enzyme in reactions catalyzing the cleavage of a substrate peptide in a time-resolved fluorescence format. Briefly, the assay was performed in a final volume of 100 µl in assay buffer containing 50 mM HEPES, pH 7.5, 150 mM NaCl, 15% glycerol, 0.15% Triton X-100, 10 mM DTT, and 0.1% PEG 8000. NS3 protease was pre-incubated with various concentrations of inhibitors in DMSO or DMSO control for 30 min at room temperature. The reaction was initiated by adding peptide substrate (final concentration 100 nM). The reaction was quenched after 1 hour at room temperature with 100 µl of 500 mM MES, pH 5.5. Product fluorescence was detected in time resolved mode with excitation at 340 nm and emission at 615 nm.

NS5B polymerase activity assay. RNA polymerase activity was assessed essentially as described in Carroll *et al.*[53] except that polymerase activity was determined in reactions catalyzed by NS5BΔ21 (genotype 1b). The activity assay involved measuring the incorporation of ^{3}H-UTP homopolymeric PolyA/OligoU template/primer, and reaction conditions included 5 nM NS5BΔ21 containing 20 mM Tris pH 7.5, 10 mM NaCl, 2 mM $MgCl_2$, 0.01% Triton, 1 mM DTT, 1 µg/0.5 µM PolyA/Oligo U_{18}, and 10 µM ^{3}H-UTP.

SCD enzymatic activity assay. HepG2 and Huh7 cells as well as Huh7 cells co-expressing genotype 1b and luciferase were used for SCD activity assays. Cells were harvested with trypsinization and subsequently quenched with complete media and then passed through a 70 µm cell strainer. Cells were centrifuged at 800 rpm for 5 minutes and then resuspended in fresh media to 200,000 cells/ml. Cells were transferred at 80 µl per well to 96-well plates (Costar 3595) and incubated at 37°C and 5% CO_2. After overnight incubation, 10 µl of compound or DMSO control in DMEM media/5% DMSO was transferred to each well and the plates were incubated at 37°C and 5% CO_2. Fifteen minutes later, 10 µl of a sonicated media containing ^{14}C-stearic acid (final concentration 0.4 µCi/ml) was added to each well and plates were incubated for 4 hours at 37°C and 5% CO_2. Cells monolayers were washed with PBS and subsequently lysed by incubation at 65°C for 1 h with 2N NaOH. Cell lysates were acidified with phosphoric acid, and lipids were extracted with acetonitrile.

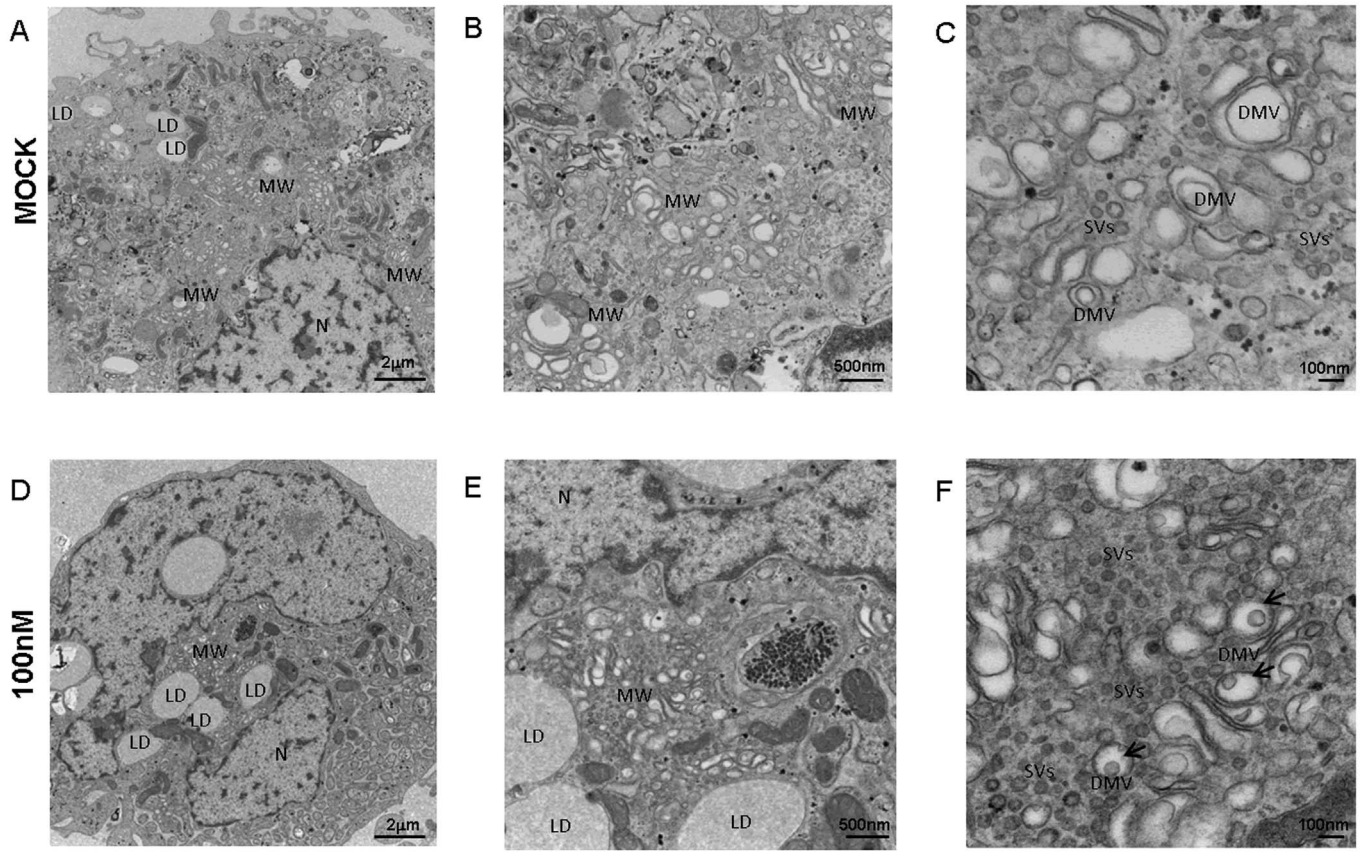

Figure 8 | Electron microscopy shows that low dose treatment with inhibitor A decreases the number of membranous webs and alters their structure while having no effect on lipid droplets in Huh7-SGR cells. Huh7-SGR cells treated for 96 h with vehicle (DMSO) (A–C) or 100 nM inhibitor **A** (D–F) were fixed and processed for EM. One representative cell is shown for each treatment at magnifications of 1500× (A), (D), 5000× (B), (E) and 15000× (C), (F). Treated cells generally showed more distortions in the double membrane vesicles, as shown by the black arrows. Treated cells also showed more small vesicles relative to control Huh7-SGR cells. MW: membranous webs, LD: lipid droplets, N: nucleus, DMV: double membrane vesicles, SVs: small vesicles, Arrows: reduction in inner membrane of DMVs.

Radiolabeled oleic and stearic acid were quantified by HPLC using a C18-reverse phase column (Zorbax extended C18 (4.6 mm × 75 mm), eluting with a 3% water (0.1% formic acid)/acetonitrile to 97% at a flow rate of 2 mL/min in 4 min, with detection via a Packard Flow scintillation analyzer.

Coherent anti-Stokes Raman scattering (CARS) imaging and quantitative voxel analysis. The CARS microscopy system uses a single femtosecond Ti:sapphire oscillator as the excitation source, as previously described[28,30]. At confluency between 20–30%, Huh7 and Huh7 SGR cells (described above) were treated with a serial dilution of inhibitor **A** (1 mM–10 nM) and inhibitor **B** (1 mM–10 nM) for a 96 hour incubation period. A total volume of media used was 2 mL for each Lab-Tek chamber (VWR, Radnor, PA, USA) for CARS imaging. Quantitative data from the CARS images was determined using a voxel counting routine in ImageJ as previously described[30,54]. After collecting multiple images for the treated samples, the average lipid volume based on voxel counting was analyzed from several cells within the same field of view.

Immunofluorescence. Huh7 cells harboring the HCV subgenomic replicon (Huh7 SGR) were seeded at 8.0×10^4 cells/well in DMEM on coverslips in a 12-well plate. After 24 h, at a confluency of 25%–30%, cells were treated with inhibitor **A** for 96 h. After inhibitor **A** treatments, cells were washed once with PBS pH 7.4 and fixed with precooled 100% methanol for 10 min at −20°C. Cells were washed three times with 1× PBS and incubated for 1 h at room temperature with a mouse monoclonal antibody specific for dsRNA (J2, 1 : 300 dilution in PBS, Scicons, Hungary). After three more washes with PBS, cells were incubated with Cy2-labeled donkey anti-mouse IgG secondary antibody (1 : 1000 dilution in PBS, Jackson ImmunoResearch Laboratories, Inc., Westgrove, PA) for 1 h at room temperature. Following three more washes with 1× PBS, cells were rinsed in H2O before being mounted onto slides with 50% glycerol in PBS. Cells images were captured using an Olympus IX81 inverted microscope (Olympus America Inc.) and fluorescence was detected through a 100× NA 1.40 oil objective. The images were analyzed using ImagePro software (MediaCybernatics) and ImageJ.

RNAse protection assay. The RNAse protection assay was adapted from Miyanari *et al.*[31]. After 96 hours of mock or inhibitor **A** treatment, Huh7 SGR cells in 60 mm cell culture plates (maintained as described above) were washed once with cold buffer B (20 mM HEPES-KOH (pH 7.7), 110 mM potassium acetate, 2 mM magnesium acetate, 1 mM EGTA, and 2 mM dithiothreitol). For selected samples undergoing digitonin (Sigma-Aldrich, Oakville, ON) treatment, buffer B containing 50 μg/ml of digitonin was added to cells for 5 min at 27°C. The reaction was stopped by washing twice with cold buffer B. For samples treated with micrococcal nuclease (MJS Biolynx, Brockville, ON) and/or NP-40 substitute (octyl I phenoxypolyethoxyethanol; Bioshop Canada Inc., Burlington, ON), the cells were washed twice with buffer D ((20 mM HEPES-KOH (pH 7.7), 110 mM potassium acetate, 2 mM magnesium acetate, 2 mM dithiothreitol, and 1 mM $CaCl_2$)) and treated with buffer D containing 0.1 unit/mL micrococcal nuclease, with or without, 0.45% NP-40 substitute for 15 min at 37°C. Samples treated with 0.45% NP-40 substitute only were incubated for 10 min at 37°C.

Total RNA was extracted using the RNeasy Mini Kits (Qiagen, Germantown, MD). The RNA integrity was assessed by electrophoresis on a 0.8% agarose, 1× TBE gel (Ambion, Austin, TX). 250 ng of total RNA was reverse transcribed into cDNA using the Superscript II Reverse Transcriptase kit (Invitrogen). Hexamers and dNTPs were purchased from Applied Biosystems. Using equal amounts of cDNA, 18S rRNA and HCV were amplified on an iCycler (Bio-Rad) using iQ SYBR Green Supermix (Bio-Rad), as per the manufacturer's protocol. The primer sequences for 18S rRNA are described in the Supplementary Table S3. Various cycle numbers were assessed to determine the cycling conditions for sub-saturating levels of the amplicon to ensure exponential amplification. The resulting amplified genes were visualized by electrophoresis on a 2% agarose 1× TAE gel. Densitometry was calculated using Image J 1.45S[55].

HCV infection and titering. JFH-1_T infection of Huh7.5 cells were performed in 6-well plates. In brief, cells were seeded with 2×10^5 cells per well. 24 hours later, cells were either infected with JFH-1_T (MOI = 0.1) or mock infected. 4 hrs post-infection (or mock infection), medium was removed and replaced with fresh medium (the normal DMEM + 10% FCS). Cells were harvested for RNA isolation 72 hours post-infection. To calculate infectious titres, supernatants were passed through a Millex-HV 45-μm filter (Millipore) before being serially diluted 10-fold in DMEM. One day prior to infection, 8-well Lab-Tek chamber slides were seeded with 5×10^4 Huh7.5 cells/well and incubated overnight. 24 hrs later, 100 μl of each infectious

dilution was used to infect chamber slides for 4 hrs before the supernatants were removed and replaced with fresh DMEM. 72 hrs post-infection, chamber slides were fixed with acetone and cells were stained using an antibody directed against core (B2; Anogen, Mississauga, Canada).

Statistical analysis. Statistical significance of difference in HCV expression levels was assessed using the paired student t-test using GraphPad Prism 4.01 (GraphPad Software Inc., La Jolla, CA).

Electron microscopy. Huh7 SGR cells were treated with vehicle (DMSO), 100 nM or 500 nM inhibitor **A** in antibiotic-free media for 96 h. Cells were fixed with 2.5% glutaraldehyde in PBS at pH 7.4. The cell pellet was resuspended in 22% BSA in PBS, recentrifuged and the resulting pellet was cut into 1 mm pieces. Samples were post-fixed in 1% osmium tetroxide in 0.1 M Na cacodylate buffer, *en bloc* stained in 3% aqueous uranyl acetate, dehydrated in ascending ethanol and embedded in Spurr epoxy resin. Ultra-thin sections were cut on a Leica EM UC6 ultramicrotome. Sections were then stained with 1% lead citrate. Digital images were taken using a JEOL 1230 TEM adapted with a 2000 by 2000 pixel bottom mount CCD digital camera (Hamamatsu, Japan) and AMT software.

1. Sakamoto, H. *et al*. Host sphingolipid biosynthesis as a target for hepatitis C virus therapy. *Nat. Chem. Biol.* **1**, 333–337 (2005).
2. Reiss, S. *et al*. Recruitment and activation of a lipid kinase by hepatitis C virus NS5A is essential for integrity of the membranous replication compartment. *Cell Host Microbe* **9**, 32–45 (2011).
3. Miller, S. & Krijnse-Locker, J. Modification of intracellular membrane structures for virus replication. *Nat. Rev. Microbiol.* **6**, 363–374 (2008).
4. Novoa, R., Calderita, G., Arranz, Ro., Fontana, J., Granzow, H. & Risco, C. Virus factories: associations of cell organelles for viral replication and morphogenesis. *Biol. Cell* **97**, 147–172 (2005).
5. Mackenzie, J. Wrapping things up about virus RNA replication. *Traffic* **6**, 967–977 (2005).
6. Tolonen, N., Doglio, L., Schleich, S. & Krijnse Locker, J. Vaccinia virus DNA replication occurs in endoplasmic reticulum-enclosed cytoplasmic mini-nuclei. *Mol. Biol. Cell* **12**, 2031–2046 (2001).
7. Wolk, B., Büchele, B., Moradpour, D. & Rice, C. A dynamic view of hepatitis C virus replication complexes. *J. Virol.* **82**, 10519–10531 (2008).
8. Lavanchy, D. Evolving epidemiology of hepatitis C virus. *Clin. Microbiol. Infect.* **17**, 107–115 (2011).
9. Miyanari, Y. *et al*. The lipid droplet is an important organelle for hepatitis C virus production. *Nat. Cell Biol.* **9**, 1089–1097 (2007).
10. Lee, W., Ishikawa, M. & Ahlquist, P. Mutation of host delta9 fatty acid desaturase inhibits brome mosaic virus RNA replication between template recognition and RNA synthesis. *J. Virol.* **75**, 2097–2106 (2001).
11. Diaz, A., Wang, X. & Ahlquist, P. Membrane-shaping host reticulon proteins play crucial roles in viral RNA replication compartment formation and function. *Proc. Natl. Acad. Sci. USA* **107**, 16291–16296 (2010).
12. Stubbs, C. & Smith, A. The modification of mammalian membrane polyunsaturated fatty acid composition in relation to membrane fluidity and function. *Biochim. Biophys. Acta* **779**, 89–137 (1984).
13. Hac-Wydro, K. & Wydro, P. The influence of fatty acids on model cholesterol/phospholipid membranes. *Chem. Phys. Lipids* **150**, 66–81 (2007).
14. Funari, S. S., Barceló, F. & Escribá, P. Effects of oleic acid and its congeners, elaidic and stearic acids, on the structural properties of phosphatidylethanolamine membranes. *J. Lipid Res.* **44**, 567–575 (2003).
15. Ntambi, J. Regulation of stearoyl-CoA desaturase by polyunsaturated fatty acids and cholesterol. *J. Lipid Res.* **40**, 1549–58 (1999).
16. Paton, C. & Ntambi, J. Biochemical and physiological function of stearoyl-CoA desaturase. *Amer. J. Physiol. Endocrinol. Metab.* **297**, E28–37 (2009).
17. van Meer, G., Voelker, D. & Feigenson, G. Membrane lipids: where they are and how they behave. *Nat. Rev. Mol. Cell Biol.* **9**, 112–124 (2008).
18. Nohturfft, A. & Zhang, S. Coordination of lipid metabolism in membrane biogenesis. *Annu. Rev. Cell Dev. Biol.* **25**, 539–566 (2009).
19. Pezacki, J., Singaravelu, R. & Lyn, R. Host-virus interactions during hepatitis C virus infection: a complex and dynamic molecular biosystem. *Mol. BioSyst.* **6**, 1131–1142 (2010).
20. Ramtohul, Y. K. *et al*. SAR and optimization of thiazole analogs as potent stearoyl-CoA desaturase inhibitors. *Bioorg. Med. Chem. Lett.* **20**, 1593–1597 (2010).
21. Isabel, E. *et al*. Biological activity and preclinical efficacy of azetidinyl pyridazines as potent systemically-distributed stearoyl-CoA desaturase inhibitors. *Bioorg. Med. Chem. Lett.* **21**, 479–483 (2011).
22. Leger, S. *et al*. Synthesis and biological activity of a potent and orally bioavailable SCD inhibitor (MF-438). *Bioorg. Med. Chem. Lett.* **20**, 499–502 (2010).
23. Powell, D. A. *et al*. Nicotinic acids: Liver-targeted SCD inhibitors with preclinical anti-diabetic efficacy. *Bioorg. Med. Chem. Lett.* **21**, 7281–7286 (2011).
24. Oballa, R. M. *et al*. Development of a Liver-Targeted Stearoyl-CoA Desaturase (SCD) Inhibitor (MK-8245) to Establish a Therapeutic Window for the Treatment of Diabetes and Dyslipidemia. *J. Med. Chem.* **54**, 5082–5096 (2011).
25. Brown, A. N. *et al*. Pharmacodynamic Analysis of a Serine Protease Inhibitor, MK-4519, against Hepatitis C Virus Using a Novel In Vitro Pharmacodynamic System. *Antimicrob. Agents Chemother.* **56**, 1170–1181 (2012).
26. Russell, R. S. *et al*. Advantages of a single-cycle production assay to study cell culture-adaptive mutations of hepatitis C virus. *Proc. Natl. Acad. Sci. USA*. **105**, 4370–4375 (2008).
27. Martin, S. & Parton, R. Lipid droplets: a unified view of a dynamic organelle. *Nat. Rev. Mol. Cell Biol.* **7**, 373–378 (2006).
28. Pegoraro, A. *et al*. Optimally chirped multimodal CARS microscopy based on a single Ti:sapphire oscillator. *Optics Exp.* **17**, 2984–3080 (2009).
29. Pezacki, J. *et al*. Chemical contrast for imaging living systems: molecular vibrations drive CARS microscopy. *Nat. Chem. Biol.* **7**, 137–145 (2011).
30. Lyn, R. K. *et al*. Direct imaging of the disruption of hepatitis C virus replication complexes by inhibitors of lipid metabolism. *Virology* **394**, 130–142 (2009).
31. Miyanari, Y., Hijikata, M., Yamaji, M., Hosaka, M., Takahashi, H. & Shimotohno, K. Hepatitis C virus non-structural proteins in the probable membranous compartment function in viral genome replication. *J. Biol. Chem.* **278**, 50301–50308 (2003).
32. Shi, S., Lee, K., Aizaki, H., Hwang, S. B. & Lai, M. M. C. Hepatitis C virus RNA replication occurs on a detergent-resistant membrane that cofractionates with caveolin-2. *J. Virol.* **77**, 4160–4168 (2003).
33. Paul, D. & Bartenschlager, R. Architecture and biogenesis of plus-strand RNA virus replication factories. *World J. Virol.* **2**, 32–48 (2013).
34. Binder, M. *et al*. Replication Vesicles are Load- and Choke-Points in the Hepatitis C Virus Lifecycle. *PLoS Pathog.* **9**, e1003561 (2013).
35. Alvisi, G., Madan, V. & Bartenschlager, R. Hepatitis c virus and host cell lipids: An intimate connection. *RNA Biol.* **8**, 258–269 (2011).
36. Herker, E. & Ott, M. Unique ties between hepatitis C virus replication and intracellular lipids. *Trends Endocrinol. Metab.* **22**, 241–248 (2011).
37. Paul, D., Hoppe, S., Saher, G., Krijnse-Locker, J. & Bartenschlager, R. Morphological and Biochemical Characterization of the Membranous Hepatitis C Virus Replication Compartment. *J. Virol.* **87**, 10612–10627.
38. Waris, G., Felmlee, D., Negro, F. & Siddiqui, A. Hepatitis C virus induces proteolytic cleavage of sterol regulatory element binding proteins and stimulates their phosphorylation via oxidative stress. *J. Virol.* **81**, 8122–8130 (2007).
39. Kim, K. H. *et al*. HCV core protein induces hepatic lipid accumulation by activating SREBP1 and PPARγ. *Biochem. Biophys. Res. Comm.* **355**, 883–888 (2007).
40. Singaravelu, R. *et al*. Hepatitis C virus induced up-regulation of microRNA-27: A novel mechanism for hepatic steatosis. *Hepatology.* **59**, 98–108 (2014).
41. Dharancy, S. *et al*. Impaired expression of the peroxisome proliferator-activated receptor alpha during hepatitis C virus infection. *Gastroenterology.* **128**, 334–342 (2005).
42. Yamaguchi, A. *et al*. Hepatitis C virus core protein modulates fatty acid metabolism and thereby causes lipid accumulation in the liver. *Dig. Dis. Sci.* **50**, 1361–1371 (2005).
43. Lerat, H. *et al*. Hepatitis C Virus Proteins Induce Lipogenesis and Defective Triglyceride Secretion in Transgenic Mice. *J. Biol. Chem.* **284**, 33466–33474 (2009).
44. Miyoshi, H. *et al*. Pathogenesis of lipid metabolism disorder in hepatitis C: Polyunsaturated fatty acids counteract lipid alterations induced by the core protein. *J. Hepatol.* **54**, 432–438 (2011).
45. Su, A. *et al*. Genomic analysis of the host response to hepatitis C virus infection. *Proc. Natl. Acad. Sci. USA*. **99**, 15669–15674 (2002).
46. Yang, W. *et al*. Fatty acid synthase is up-regulated during hepatitis C virus infection and regulates hepatitis C virus entry and production. *Hepatology* **48**, 1396–1403 (2008).
47. Nasheri, N. *et al*. Modulation of Fatty Acid Synthase Enzyme Activity and Expression during Hepatitis C Virus Replication. *Chem. Biol.* **20**, 570–582.
48. Lachance, N. *et al*. Discovery of potent and liver-targeted stearoyl-CoA desaturase (SCD) inhibitors in a bispyrrolidine series. *Bioorg. Med. Chem. Lett.* **22**, 980–984 (2012).
49. Livak, K. & Schmittgen, T. Analysis of relative gene expression data using real-time quantitative PCR and the $2^{-\Delta\Delta Ct}$ Method. *Methods* **25**, 402–408 (2001).
50. Vrolijk, J. M. *et al*. A replicon-based bioassay for the measurement of interferons in patients with chronic hepatitis C. *J. Virol. Methods* **110**, 201–209 (2003).
51. Dhanak, D. *et al*. Identification and Biological Characterization of Heterocyclic Inhibitors of the Hepatitis C Virus RNA-dependent RNA Polymerase. *J. Biol. Chem.* **277**, 38322–38327 (2002).
52. Mao, S.-S. *et al*. A time-resolved, internally quenched fluorescence assay to characterize inhibition of hepatitis C virus nonstructural protein 3-4A protease at low enzyme concentrations. *Anal. Biochem.* **373**, 1–8 (2008).
53. Carroll, S. S. *et al*. Inhibition of Hepatitis C Virus RNA Replication by 2′-Modified Nucleoside Analogs. *J. Biol. Chem.* **278**, 11979–11984 (2003).
54. Lyn, R. K., Kennedy, D. C., Stolow, A., Ridsdale, A. & Pezacki, J. P. Dynamics of lipid droplets induced by the hepatitis C virus core protein. *Biochem. Biophys. Res. Comm.* **399**, 518–524 (2010).
55. Schneider, C., Rasband, W. & Eliceiri, K. NIH Image to ImageJ: 25 years of image analysis. *Nat. Methods* **9**, 671–675 (2012).

Acknowledgments

This work was supported by a grant from the Canadian Institutes of Health Research (CIHR) and Natural Sciences and Engineering Research Council (NSERC) of Canada. RKL

thanks the NSERC CREATE program in Medicinal Chemistry and Biopharmaceutical Development for support and training. RS thanks NSERC for a Vanier Graduate Scholarship and the CIHR National Canadian Research Training Program in Hepatitis C for additional support and training. A.P. and S.K. would like to thank H. Wang, M. Henault, S. Radinovic, E. Mulrooney, S. Gagné, and J. Vaillancourt for fruitful discussions. JPP would like to thank A. Stolow (NRC) for many fruitful discussions and collaborations in CARS microscopy.

Author contributions

J.P.P. and A.P. contributed in conception and design, data analysis and interpretation, and manuscript writing. R.K.L. contributed in conception and design, collection and assembly of data, data analysis and interpretation, and aided in the preparation of the manuscript. R.S., S.K., S.O., H.C., R.O., Z.H., A.R., R.S.R. and D.M.J. contributed in collection and assembly of the data, data analysis and interpretation, and aided in the preparation of the manuscript.

Additional information

Supplementary information accompanies this paper at http://www.nature.com/scientificreports

Competing financial interests: The authors declare no competing financial interests.

How to cite this article: Lyn, R.K. *et al.* Stearoyl-CoA desaturase inhibition blocks formation of hepatitis C virus-induced specialized membranes. *Sci. Rep.* **4**, 4549; DOI:10.1038/srep04549 (2014).